

# The Turbo-Charged Mapper: Fast and Optimal Mapping for Accelerator Modeling and Evaluation

Michael Gilbert\*  
 MIT  
 Cambridge, MA, USA  
 gilbertm@mit.edu

Tanner Andrulis\*  
 MIT  
 Cambridge, MA, USA  
 andrulis@mit.edu

Vivienne Sze  
 MIT  
 Cambridge, MA, USA  
 sze@mit.edu

Joel S. Emer  
 MIT / Nvidia  
 Cambridge, MA, USA  
 emer@csail.mit.edu

**Abstract**—The energy and latency of an accelerator running a deep neural network (DNN) depend on how the computation and data movement are scheduled in the accelerator (*i.e.*, *mapping*). Optimizing mappings is essential to evaluating and designing accelerators. However, the space of mappings is large, and prior works can not guarantee finding optimal mappings because they use heuristics or metaheuristics to narrow down the space. These limitations preclude proper hardware evaluation, since designers can not tell whether performance differences are due to changes in hardware or suboptimal mapping.

To address this challenge, we propose the Turbo-Charged Mapper (TCM), a fast mapper that is guaranteed to find optimal mappings. The key to our approach is that we define a new concept in mapping, called *dataplacement*, which, like the prior concept of dataflow, allows for clear analysis and comparison of mappings. Through it, we identify multiple opportunities to prune redundant and suboptimal mappings, reducing search space by up to 32 orders of magnitude.

Leveraging these insights, TCM can perform full mapspace searches, making it the first mapper that can find optimal mappings in feasible runtime. Compared to prior mappers, we show that TCM can find optimal mappings quickly (less than a minute), while prior works can not find optimal mappings (energy-delay-product 21% higher than optimal) even when given  $1000\times$  the runtime ( $> 10$  hours).

**Index Terms**—Deep Neural Networks, Systems, Hardware, Modeling, Mapping

## I. INTRODUCTION

The design and analysis of a deep neural network (DNN) accelerator requires optimizing how computation and data movement are scheduled onto the accelerator (*i.e.*, the *mapping* [1]–[5]) to minimize latency and energy [1]. This optimization is done using a *mapper* [1], which must explore a very large space of mappings (*i.e.*, the *mapspace* [1]), containing as many as  $10^{37}$  mappings<sup>1</sup>. Given the infeasibility of evaluating every mapping, prior mappers [1], [3], [4], [7]–[9] use heuristics (*e.g.*, only evaluate mappings that maximize buffer utilization) or metaheuristics (*e.g.*, randomly sample different mappings), which speed up mapspace search but cannot guarantee finding an *optimal* mapping. *Optimal* means

\*These authors contributed equally to this work

TCM is integrated into the AccelForge framework, available at <https://accelergy-project.github.io/accelforge/>. Please direct all questions on this work to AccelForge.

<sup>1</sup>Mapping counts in this section are from GPT-3 [6] Einsum *QK* in Section VI-B. Counts depend on workload, architecture, and mapspace.

that, in the defined mapspace, there is no valid (*i.e.*, within resource limits) mapping with superior objective metrics (*e.g.*, energy).<sup>2</sup>

To address this challenge, we introduce new strategies that can prune suboptimal mappings from the mapspace. These strategies reduce search size by up to 32 orders of magnitude while guaranteeing that we find the optimal mapping. These pruning strategies leverage new mapping analyses, enabled by a new concept called *dataplacement*.

Dataplacement, alongside *tile shapes* and *dataflow*, together comprise a mapping. Prior work has defined *tile shapes* as the size and number of tiles that subdivide workload data (tensors), and *dataflow* as the traversal of tiles in space/time [1]–[4], [7].

Dataplacement, defined in this work, completes the mapping by specifying which tiles are kept at a given point in time in each memory level of the accelerator. Dataplacement enables fast mapspace exploration for two reasons. First, we can use information provided by dataplacement to prune suboptimal dataflows ( $10^{15} \rightarrow 1$ ) and tile shapes ( $10^{22} \rightarrow 10^5$ ). Second, there are very few dataplacements (only 16) relative to dataflows ( $10^{15}$ ) and tile shapes ( $10^{22}$ ), so we can fully explore the dataplacement space, then prune before exploring dataflows and tile shapes. Specifically, we use information from dataplacement in two ways.

First, dataplacement shows which tiles are stored in each memory level, and there are dataflows and tile shapes that unnecessarily re-fetch these tiles, or keep larger-than-needed tiles. We identify and prune these suboptimal dataflows ( $10^{15} \times$  reduction) and tile shapes ( $10^{10} \times$  reduction).

Second, dataplacement and dataflow determine qualitative information about tiles (“what”, “where”, and “when”), while tile shapes affect only quantitative information (“how big” and “how many”). This means that most of the modeling complexity is in dataplacement and dataflow. In fact, for a given dataplacement and dataflow, accesses, energy, and latency can be calculated using functions of simple, easy-to-reason-about operators (*e.g.*, multiply, add, min, ceiling), which lets us reason about these functions to find tile shape choices that dominate others ( $10^6 \times$  reduction). After generating these

<sup>2</sup>We also consider redundant mappings (*i.e.*, identical metrics to an unpruned optimal mapping) to be suboptimal. While the optimal definition is mapspace-dependent, our optimality-guaranteed mapspace is a superset of the mapspaces of many prior works [1], [2], [7]–[10].

simple functions, we can also evaluate them instead of running a full model to speed up the search process by  $> 100\times$ .

We implement these ideas in the Turbo-Charged Mapper (TCM), which fully searches the mapspace, making it the first mapper to guarantee finding optimal mappings in feasible runtime (seconds to minutes). We also compare to prior works that trade off optimality for speed [1], [7], [9], showing that, given similar runtime, this work finds mappings with  $1.3 - 2400\times$  lower EDP.

In summary, we make the following contributions:

- We introduce the concept of dataplacement that defines which tiles are stored in each level of the memory hierarchy. Dataplacement clearly shows the relative sizes and lifetimes of each tile in memory.
- We show how to use dataplacement to identify and prune suboptimal dataflows and tile shapes.
- We introduce *partial-tile-shape-pruning*, which, for a given dataplacement and dataflow, can identify and prune suboptimal tile shapes.
- We introduce a fast model that is compiled once for each dataplacement and dataflow, and is then  $1000\times$  faster than prior fast models.
- We integrate these contributions into TCM, the first mapper to guarantee finding optimal mappings in feasible runtime. TCM fully searches the mapspace, pruning only suboptimal mappings.

## II. BACKGROUND

### A. Einsum Notation

We describe DNN computations (e.g., matrix multiplications, convolutions, activation functions) using the *Einsum notation*. In the Einsum notation, each multi-dimensional data is referred to as a *tensor* and its dimensions (e.g., channels in a feature map) as *ranks*. Valid coordinates in that rank (e.g., channels 0 through 2) are the *shape* of the rank<sup>3</sup>, and the shapes of ranks in a tensor are collectively referred to as the tensor's shape.

Einsums are written like sums, but omit the sum symbol and write index expressions as subscripts. For example, consider the matrix multiplication where *rank variables*  $m, k$ , and  $n$  index into tensors  $A$ ,  $B$ , and  $Z$ . Written as an Einsum, we make implicit the summation over  $k$  (in general, we sum over all variables not present in the equation's left-hand side):

$$\text{Sum: } Z[m, n] = \sum_k A[m, k] \times B[k, n] \quad (1)$$

$$\text{Einsum: } Z_{m, n} = A_{m, k} \times B_{k, n}$$

### B. Mappings in LoopTree Notation

A *mapping* schedules, in space and time, a workload's computation steps and all operations in them [1], [11], [12]. This paper represents mappings with *LoopTrees* [5], [13], which clearly show mapping choices and their consequences.

<sup>3</sup>Coordinates in all ranks in this paper start with index 0, so we specify the exclusive upper-bound as the shape. For example, shape 3 denotes  $\{0, 1, 2\}$ .

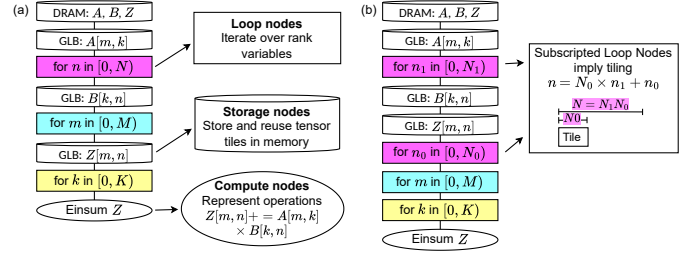


Fig. 1. (a) An example LoopTree, the different types of nodes, and their meaning. (b) An example LoopTree with tiling.

Fig. 3(a) shows an example mapping as a LoopTree for the Einsum in Eq. 1. LoopTrees consist of:

- *Loop nodes*, rectangles in the LoopTree, represent nested `for` loops that iterate over rank variables in the workload. Multiple loops over a rank variable imply tiling, and subscripts indicate iteration over tiles and within tiles (e.g., in Fig. 3(a), the loop over  $m_1$  iterates over tiles, the loop over  $m_0$  iterates within a tile, and we index with  $m = m_1 M_0 + m_0$ ).
- *Storage nodes*, cylinders in the LoopTree, represent tensor tile storage. Each tile's size is determined by the loops below the storage node (e.g., Fig. 3(a) and (b) show that the GLB  $A$  storage node must keep a  $K_0 \times M_0$  tile). The number of tiles fetched (including refetches) is determined by the loops above the storage node (e.g., in Fig. 3(a), the  $A$  tile in GLB is fetched  $M_1 K_1$  times).
- *Compute nodes*, ovals in the LoopTree, represent the computation that is performed. In this example, they represent the multiply-accumulate operations in the Einsum. To complete the terminology:
  - *Dataflow* is the relative ordering of operations, which in LoopTree notation is the loop nodes and their order.
  - *Tile shapes* are the shape of tiles in each rank, which in LoopTree notation are the loop bounds.
  - *Dataplacement* is the tensor tiles that are held in memory levels, which in LoopTree is the storage nodes and their order. Section III discusses more details.

### C. Challenges in Mapspace Exploration

Finding optimal mappings requires a mapping search, as there is no known direct solver. This is because hardware is complex, and each mapping choice impacts many factors (e.g., parallelism, bandwidth utilization, capacity utilization), which then affect final energy and latency.

Mapspace search is challenging because the mapspace is very large. Only a very small fraction of the mapspace can be evaluated within a feasible runtime, even with the fastest models [1]–[5], [7]. Then, the challenge is determining which mappings out of the mapspace should be evaluated to find the best mapping possible.

### D. Constructing, Sizing, and Pruning The Mapspace

We can construct the mapspace by making a series of decisions: picking a dataplacement, a dataflow, and then tile

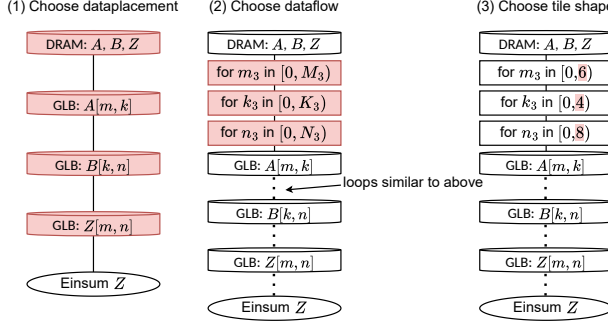


Fig. 2. Constructing a mapspace for the Einsum in Eq. 1 by choosing dataplacement, dataflow, then tile shape. The part of the mapping chosen in each step is highlighted in red. In (2) and (3), only some choices are shown; similar choices must be made for parts in ellipses.

shapes. Fig. 2 illustrates this process. (1) We choose a dataplacement  $dp \in DP$ , which is the order of storage nodes and whether to include them (e.g., whether to keep tensor  $I$  in GLB). Storage nodes for different tensors can be reordered freely, but storage nodes must follow memory hierarchy order (e.g., DRAM has to be above GLB)<sup>4</sup>. It is also common to have only one storage node for the highest memory level (e.g., DRAM) that stores every tensor in entirety. (2) loops over every rank variable are placed between every pair of adjacent two storage nodes, and we choose a dataflow  $df \in DF$ , which is the choice of loop orders. (3) we choose tile shapes  $ts \in TS$ , which are the loop bounds. Following this process, the mapspace size is:

$$|\text{Mapspace}| = |DP| \cdot |DF| \cdot |TS| \quad (2)$$

The number of options varies significantly across different choices, and  $|DP|$  is tends to be smallest by a wide margin. The reason for this can be seen in Fig. 2; there are many more loops than storage nodes, making the spaces of loop orders and loop bounds much larger than the space of storage node orders. For example, mapping the attention matrix computation step in GPT-3 to a TPU-like architecture,  $|DP| = 16$ ,  $|DF| \approx 10^{15}$ , and  $|TS| \approx 10^{22}$ .

Leveraging this variation, we maximize pruning potential by focusing on reducing  $|DF|$  and  $|TS|$ . The following sections will describe how we prune dataflows when given a dataplacement choice and how we prune tile shapes given dataplacement and dataflow choices. For the same example as above,  $|DF|_{\text{pruned}} = 1$  and  $|TS|_{\text{pruned}} \approx 10^5$ , representing a 32 order of magnitude pruning rate overall.

### E. Prior Work

To manage the large mapspace, prior work has proposed various heuristics [1], [7], [9] and metaheuristics [3], [4], [14], [15], but these approaches cannot guarantee finding an optimal mapping. Heuristic approaches use simple-to-evaluate rules (e.g., maximize parallelism) to narrow down which

<sup>4</sup>TCM can optionally relax this assumption, making the memory hierarchy constraint per-tensor (e.g., (GLB, input) storage node must go above (register, input) storage node, but may be below (register, output) storage node).

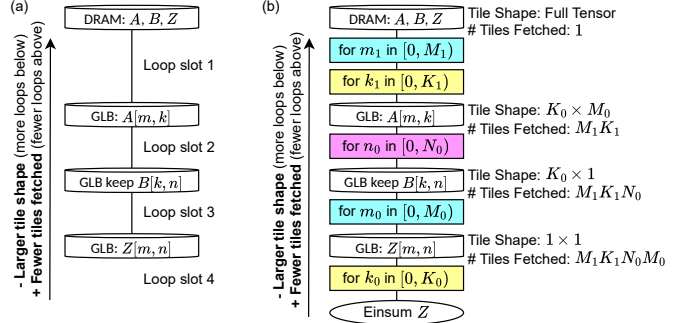


Fig. 3. (a) An example dataplacement and slots where loops may be inserted. (b) An example mapping using the dataplacement, including tile shapes and numbers of tiles fetched. Dataplacement shows the trade-off between tile size and number of tiles fetched: Storage nodes higher in the dataplacement reduce fetches, but can increase tile size.

mappings to evaluate. However, these rules only capture some of the factors that determine latency and energy, and ignore important trade-offs. For example, increasing parallelism can result in more memory accesses and, when bandwidth is limited, increase latency instead.

Prior mappers also use metaheuristics such as sampling [1], genetic algorithms [3], [14], Bayesian optimization [15], simulated annealing [4], and Monte Carlo Markov chains [16]. However, while these approaches yield better-than-random results, they have no guarantee of finding the optimal mapping.

While some prior works include optimality-preserving pruning techniques for dataflows [7], [8], without prior knowledge of the dataplacement, this pruning is less effective than ours, and these works still need heuristics to search the mapspace.

### III. DEFINING AND INTERPRETING DATAPLACEMENT

First, we precisely define dataplacement, how we specify it in the LoopTree notation, and its impact on data reuse.

#### A. Understanding and Specifying Dataplacement

*Dataplacement*, which determines the tensor tiles present in each memory level, is represented in the LoopTree notation as storage nodes and their ordering. Existence of a storage node implies whether a tile is stored (e.g., a storage node “GLB keep  $A$ ” says the GLB keeps tiles of Tensor  $A$ ), and storage node order affects tile shapes, how long tiles live (i.e., their *lifetimes*), and the amount of reuse.

Fig. 3 shows how dataplacement affects tile shapes, lifetime, and reuse. Fig. 3(a) shows the dataplacement alone, while Fig. 3(b) shows a full LoopTree, which includes loops inserted into slots between storage nodes. The dataplacement enforces two invariants on the lifetime and shape of stored tiles:

*Invariant 1: Storage nodes higher in the dataplacement have the same-or-longer lifetime than those lower in the dataplacement.* For example, the “GLB keep  $A$ ” storage node in Fig. 3(b) is alive for the iterations of all loops in slots 2, 3, and 4; while the “GLB keep  $Z$ ” storage node below is only alive for loops in slot 4, and new tiles are fetched for each iteration of the loops in slots 2 and 3. Fig. 3(c) shows that this

results in fewer fetches, and thus more reuse, for the “GLB keep  $A$ ” storage node.

*Invariant 2: Storage nodes higher in the dataplacement have the same-or-larger shape than those lower in the dataplacement.* (Note that shape comparisons apply only to ranks shared between the stored tensors.) For example, “GLB keep  $A$ ” storage node Fig. 3(b) stores a  $K_0 \times M_0$  tile of Tensor  $A$ , while “GLB keep  $Z$ ” stores a  $K_0 \times 1$  tile. This invariant is again because higher storage nodes are above more loops than lower storage nodes, and in the LoopTree notation, the tile shape is the product of loop bounds of relevant loops under the storage node.

Increased lifetime and tile shape mean that higher storage nodes often have more reuse opportunities than lower storage nodes because tiles are kept for longer. However, only loops that have reuse opportunities will result in reuse. For example, the tile specified by “GLB keep  $A$ ” reuses data across iterations of the  $n_0$  loop, but not the  $k_0$  loop, because each  $k_0$  iteration accesses a different value of  $A$ .

### B. Dataplacement for Interpreting Mappings

Dataplacement offers new insights into how mappings use memory resources to reuse data and reduce refetches. In particular, dataplacement provides a notion of *reuse priority*, which determines the relative amount of memory resources to be used to get more reuse of different tensors.

Traditionally, hardware designers analyze reuse by looking at the dataflow, inferring how tensor tiles are reused based on the order of operations. A dataflow-centric analysis (e.g., categorizing dataflows by stationarity [11], [12], [17]) would look at all loops that exist between any two memory levels. For example, in Fig. 3, the DRAM-GLB dataflow is based on the uppermost four loops (between the DRAM storage node and the lowest GLB storage node), and the dataflow is  $B$ -stationary because the innermost of these loops, the  $m_0$  loop, repeatedly accesses the same elements of  $B[k, n]$ . Therefore, we can store and reuse  $B[k, n]$  for multiple iterations.

Analyzing mapping through the lens of dataplacement offers two new insights. First, the dataplacement shows clearly which tiles are kept in the memory longer and the relative shape of the tiles. For example, in Fig. 3, the dataplacement implies that the tile of  $A[m, k]$  is kept in GLB for longer and has a larger shape, followed by tiles of  $B[k, n]$  and  $Z[m, n]$  in order. Second, as a corollary, the dataplacement shows the *relative priority* of tensors. In our example,  $A[m, k]$  has the highest reuse priority, followed by  $B[k, n]$  and  $Z[m, n]$ .

Reuse priority provides an intuition for the benefits of the ability to specify a storage node for each tensor (also referred to as *uneven mappings* [7]), which have been shown to reduce energy and latency [5], [7]. Works that focused only on dataflow and implicitly assume a dataplacement (often placing storage nodes for all tensors at the same place) [1], [3], [8], missed this optimization because they only reuse the tensor(s) that are kept stationary for a given dataflow. For example, in Fig. 3, placing storage nodes for  $A[m, k]$  at the same level as  $GLB : Z[m, n]$  eliminates all reuse of  $A$ .

Because it provides both a clear way to interpret mappings and a richer space to explore, dataplacement is important to our understanding of mapping.

## IV. SPEEDING UP MAPPING USING DATAPLACEMENT

We show how dataplacement lets us identify and prune many dataflows, loops, and tile shapes that are guaranteed to be worse-than or equal-to the optimal choices. Then, we show how we can use dataplacement to speed up the model.

### A. Redundant Dataflow Pruning

Knowing dataplacement, we can reduce the number of mappings to evaluate by identifying redundant dataflows.

Many dataflows are redundant and do not need to be evaluated. In general, dataflows that differ only in the order of loops between the same storage nodes result in exactly the same tile shapes and data movement. For example, in Fig. 3(b), permuting the top two loops would not change tile shapes or the number of fetches. Thus, we do not need to explore orders of loops that are not separated by storage nodes.

This pruning represents significant improvement over prior dataflow explorations [1], [7], which explore all loop orders instead of exploring only non-redundant dataflows for each dataplacement. There are fewer storage nodes than loops ( $\leq 3$  storage nodes per memory level, versus 3–7 loops), leading to far fewer storage node orders than loop orders (less than  $10^3$  versus more than  $10^7$ ). Because there are few non-redundant dataflows for each dataplacement, we reduce the number of choices we must explore significantly.

The one exception to this pruning rule is if the rank variable is part of an expression in the index (e.g.,  $p$  in a convolution  $Z_p = A_{p+r} \times W_r$ ), sometimes referred to as a *partially relevant* rank variable [7]. In such cases, a loop over  $p$  directly under a storage node for  $A$  allows only a line buffer to be held in storage for  $A$ , which reduces memory requirements [1], [5], [7], [11], [18]. Such optimization is only applied to the loop directly under the storage node. Thus, when such rank variables exist, we explore loop orders that leads to a unique partially-relevant loop beneath applicable storage nodes (e.g., for  $Z_p = A_{p+r} \times W_r$ , for each  $A_{p,r}$  storage node, there is a choice to put the  $p$  loop highest or the  $r$  loop highest).

### B. Non-Helpful Loop Pruning

Knowing dataplacement, we can identify and remove loops that have no benefit but cost more data movement and/or larger memory requirements.

For example, in Fig. 4, the uppermost  $n_2$  loop is not helpful because it increases refetches of  $A$  without additional benefit. Each iteration of the  $n_2$  loop accesses the *same* tile of  $A[m, k]$ . Therefore, there is a reuse opportunity for  $A[m, k]$ . If we remove the loop (equivalent to setting  $N_2 = 1$ ), we get more  $A[m, k]$  reuse and reduce the number of  $A[m, k]$  tiles fetched from DRAM without increasing memory requirements.

The lowermost  $n_0$  loop is not helpful because it increases  $B[k, n]$  tile size (larger memory requirement) without additional benefit. Each iteration of the  $n_0$  loop accesses a

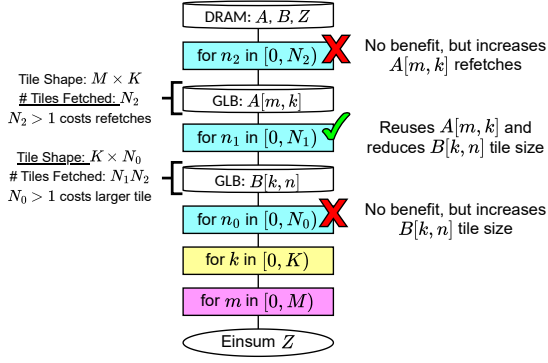


Fig. 4. A mapping with non-helpful loops. Notice that the  $n_2$  and  $n_0$  loops both have costs (more fetches, more tile size) but no benefits (lower fetches, lower tile size). The  $n_1$  loop is strictly better than either. Loop pruning will eliminate the  $n_2$  and  $n_0$  loops while keeping the  $n_1$  loop.

Reuse tensor above	Reuse tensor below	Pruned?
Yes	No	No
No	*	Yes
*	Yes	Yes

TABLE I

RULES TO PRUNE A LOOP BASED ON WHETHER IT REUSES THE TENSOR IN THE STORAGE NODE ABOVE/BELOW IT. ASTERISK (\*) MEANS ANY.

different element  $B[k, n]$ , which means that there is no reuse opportunity. Therefore, keeping multiple  $n_0$  in GLB results in a larger tile, but does not reduce the amount of data fetched from DRAM. If we remove the  $n_0$  loop, we reduce the  $B[k, n]$  tile size without increasing data movement.

In summary, we can remove loops that do not index into the tensor in the storage node below or do index into the tensor in the storage node above (see Table I).

This analysis significantly decreases the number of loops to consider. In matrix multiplications, the number of loops per storage node goes  $3 \rightarrow 1$ . For more complex workloads, the reduction is greater (e.g.,  $6 \rightarrow 2$  per storage node in our GPT-3 [6] experiments). Since the number of tile shapes (ways to factorize workload shape to loop bounds) and dataflows (orders of loops) increases exponentially with the number of loops, this pruning dramatically decreases mapspace size.

We note that ZigZag [7] includes similar observations on helpful and non-helpful loops, calling it the Loop Relevance Principle (LRP). Our analysis on whether a loop is helpful matches ZigZag's. The difference is that ZigZag uses this analysis to prune dataplaces (create a dataflow (loop nodes) first; only insert storage nodes such that the surrounding loops are helpful), while we use it to prune loops (create a dataplace (storage nodes) first; only insert helpful loops). Pruning loops is much more effective as it reduces the dataflow and tile shape space, which is much larger than the dataplace space ( $10^{10} - 10^{25}$  versus  $10 - 1000$ ).

### C. Partial Tile Shape Pruning

Hardware performance models, even analytical ones, generally involve complex calculations, but we can simplify

the model and conduct trade-off analysis if we fix certain design choices. For example, while it would be difficult to write a single expression that calculates DRAM accesses for arbitrary mappings, the number of DRAM accesses by Tensor  $B$  elements in Fig. 3 and the GLB usage of  $A$  are:

$$\begin{aligned} \text{DRAM Accesses}_B &= M_1 \cdot K \cdot N \\ \text{GLB Usage}_A &= M_0 \cdot K_0 \end{aligned} \quad (3)$$

In fact, given dataflow and dataplace, we can generate expressions for the usage and accesses to every memory level, as well as final metrics such as energy and latency.

Using these expressions, we can identify and prune sub-optimal mappings even before knowing all the tile shapes. A partially-chosen set of tile shapes can be pruned if we can show that it will result in worse metrics regardless of future tile shape choices (e.g., the tile shape along a dimension may so severely underutilize an array of computation units that it results in high latency regardless of the tile shape along other dimensions). Finding such pruning candidates requires complex analysis, which is described in Section V-D.

### D. Speeding Up Modeling via Currying

Explicit dataplace also enables much faster modeling runtime. We can compute the mathematical expressions as in the previous section first for a combination of dataflow and dataplace. Then, we use those expressions to explore various tile shapes, which is now much faster because it only involves numerical substitutions and arithmetic operations. In other words, we separate the model such that the input can be given one at a time (*i.e.*, we *curry* the model). Moreover, each mathematical expression can be used for the entire tile shape exploration. Thus, we trade off the slightly more expensive symbolic analysis of the impact of dataplace and dataflow to obtain a faster model that we can reuse for all tile shapes.

### V. THE TURBO-CHARGED MAPPER (TCM)

In this section, we describe the Turbo-Charged Mapper (TCM), which implements the ideas in Section III. TCM, shown in Fig. 5 is the first to output optimal mappings in a feasible runtime.

Optimal mappings are guaranteed because TCM only prunes choices that are known to be suboptimal. Meanwhile, when exploring at a given step, it explores every possible choice that may be optimal (*i.e.*, it does not miss anything).

TCM includes four key steps:

- Make dataplace choices. This is equivalent to making every possible ordering of storage nodes in the Loop-Tree. This step outputs a partial mapping ( $pmapping$ ), which is a mapping with only some attributes specified.
- Make dataflow choices for each dataplace choice. This step reduces mapspace size by only generating Pareto-optimal dataflows.
- Make a tile-shape-only model, which fixes dataflow and dataplace to take only tile shapes as input.
- Explore tile shapes. This uses the tile-shape-only model to explore possible tile shapes. As it chooses tile shapes, it

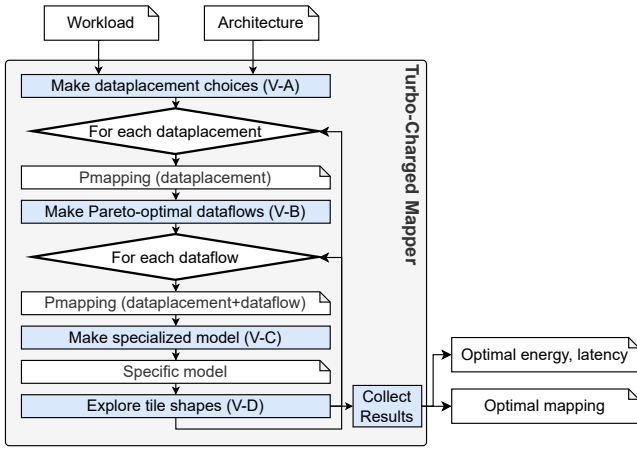


Fig. 5. Overview of TCM. Each mapper process (in blue) is explained in detail in the sections in parentheses.

will prune known-suboptimal choices to keep the search size tractable.

The four steps are detailed in the following subsections.

#### A. Making Dataplacement Choices

TCM explores all dataplacement choices, which involves making and ordering storage nodes. Making storage nodes means that we decide, for each memory level and tensor, whether to keep a tile of the tensor in the memory level (*i.e.*, whether the storage node exists). TCM generates all possible combinations of storage nodes (except those that are not supported by the hardware). Then, for each combination, TCM generates all possible hardware-supported storage node orders. Storage order must also obey the hardware memory hierarchy, meaning that we can not have the  $L1 : A[m, k]$  storage node higher than the  $L2 : A[m, k]$  storage node, else the mapping would use  $L1$  as a backing store for  $L2$ .

Users may constrain the dataplacement as well. This may be useful if a memory is used to store a particular tensor (*e.g.*, `WeightBuffer` can only hold weights).

#### B. Making Pareto-Optimal Dataflows

For each dataplacement choice, TCM explores all non-redundant dataflow choices. We first explore ordering of the loops in each slot, then all combinations of per-slot choices.

Between any two storage nodes, we determine the set of loops over rank variables that would be beneficial to insert between any two storage nodes using the principles discussed in Section IV-B. We then partition the rank variable (*e.g.*,  $n \rightarrow n_0 n_1$ ) and insert a loop between the two storage nodes. In cases where there is no lower storage node (*i.e.*, below the last storage node, above the compute node), we omit the reuse-tensor-below check. In cases where the upper storage node is the outermost backing storage (*e.g.*, DRAM) we omit the reuse-tensor-above check since loops may not be placed above this backing storage. Given the set of loops between storage nodes, we explore choices of which loop is directly under the storage node above, and we choose a canonical order (*e.g.*,

alphabetical) for the rest of the loops because the order does not matter (see Section IV-A).

#### C. Making the Tile-Shape-Only Model

Like prior work [1], [7], [9], our model takes in workload, architecture, and mapping specifications as inputs to calculate overall energy and latency. However, our model is much faster for mapping search because it performs the most time-intensive modeling work (analyzing a particular dataplacement and dataflow) a handful of times (tens to hundreds), sharing this effort across all mappings that have the same dataplacement and dataflow (thousands to millions).

To achieve this speed, our model is *curried*, meaning we first give the model dataplacement and dataflow, and it outputs a *tile-shape-only model* that only needs tile shapes as input:

$$\begin{aligned} \text{TileShapeOnlyModel} &= \text{FullModel}(\text{dataplacement}, \text{dataflow}) \\ \text{Results} &= \text{TileShapeOnlyModel}(\text{tile shapes}) \end{aligned}$$

The tile-shape-only model is simpler and faster than a full model, as it omits the complexity of dataplacement and dataflow analysis. In fact, the tile-shape-only model can calculate energy, latency, or usage of any on-chip resource using simple sum-of-product and max expressions. Given a dataplacement and dataflow, we calculate the tile size and number of accesses for Storage  $s$  with the following:

$$\begin{aligned} \text{TileSize}(s) &= \prod_{l \in \text{Indexing Loops Below}} l.\text{bound} \\ \text{TilesFetched}(s) &= \prod_{l \in \text{Loops Above}} l.\text{bound} \\ \text{AccessesToAbove}(s) &= \text{TileSize}(s) \cdot \text{TilesFetched}(s) \quad (4) \end{aligned}$$

For each memory  $m$  with storage nodes  $\text{Storage}(m)$ , we aggregate accesses and tile size:

$$\begin{aligned} \text{Usage}(m) &= \sum_{s \in \text{Storage}(m)} \text{TileSize}(s) \\ \text{Energy}(m) &= \sum_{s \in \text{Storage}(m)} \text{Accesses}(m) \cdot \text{AccessEnergy}(m) \\ \text{Latency}(m) &= \text{Accesses}(m) / \text{Bandwidth}(m) \end{aligned} \quad (5)$$

Finally, we calculate compute latency and energy, then aggregate across components:

$$\begin{aligned} \text{Latency}_{\text{Compute}} &= \text{Computes} / \text{UtilizedComputeUnits} \\ \text{Energy}_{\text{Compute}} &= \text{Computes} \cdot \text{PerComputeEnergy} \\ \text{Latency} &= \max \left( \max_{m \in \text{memories}} \text{Latency}(m), \text{Latency}_{\text{Compute}} \right) \\ \text{Energy} &= \text{ComputeEnergy} + \sum_{m \in \text{memories}} \text{Energy}(m) \quad (6) \end{aligned}$$

This model is like other analytical models [1], [10]. The expressions here are computed symbolically, forming the tile-shape-only model, which accepts numerical tile shapes to generate numerical latency and energy values. Then, complex calculations (such as finding all loops above a given storage node) resolve to simple variable substitutions.

Finally, the model we discussed is simplified for clarity; TCM’s model supports many other optimizations, including those not supported in prior work [1], [7]. These optimizations can also be modeled as sum-of-product and max expressions<sup>5</sup>.

#### D. Exploring Tile Shapes

After choosing dataplacement and dataflow, we must explore tile shapes. Concretely, we must choose numerical values for  $\text{TileShapes} = \{b_1, \dots, b_n\}$ , where each  $b_i$  is a loop bound in the mapping for which we must provide a numerical value. Because each  $b_i$  has many choices, and the full space scales exponentially with the number of loops, the full space is very large (up to more than  $10^{10}$  choices).

To address this exponential growth, we explore loop bound values for one loop at a time<sup>6</sup>, and prune our tile shape choices as we make them (*i.e.*, we want to prune *partial tile shapes*). With full tile shapes, it is straightforward to detect whether one set of tile shapes is better than another: we can simply call the model,  $\text{TileShapeOnlyModel}(b_1, \dots, b_n)$ , compare the results, and prune the worse choice. However, partial tile shapes cannot be evaluated with the model, so we create a different *pruning criteria* for partial tile shapes.

1) *Pruning Criteria for Partial Tile Shapes*: We generate the pruning criteria from the optimization objectives (*e.g.*, latency or energy), but each criterion can be evaluated using information within the partial tile shapes. Moreover, each criterion is marked as “minimize,” “maximize,” or “cannot compare.” A choice of partial shapes is better than another choice if it is better in all “maximize” and “minimize” criteria (lower in all “minimize” criterion and higher in all “maximize” criterion) and exactly matches in all “cannot compare” criteria.

To describe how we generate our pruning criteria, suppose we are in the middle of the exploration, and we have generated all possible loop bounds for loops  $\{k_1, \dots, k_m\}$ , but not for loops  $\{u_1, \dots, u_p\}$  (the known and unknown loop bounds respectively). Before we choose another loop to explore, we prune the choices we have generated (*i.e.*, the values for loops  $k_i$ ). Since we cannot fully evaluate the model (we have no numerical values for  $u_i$ ), we create various criteria  $C_i$ , which are dependent only on known tile shapes,  $C_i = C_i(k_1, \dots, k_m)$ .

We create criteria by applying rewrite rules to the  $\text{TileShapeOnlyModel}$  as starting criteria (one criterion for latency, one for energy, and one for usage of every resource). The most common rule is *partitioning* a criterion. For example, suppose we want to minimize GLB usage by tiles of tensors  $A$  and  $B$ .

$$\text{GLB Usage} = \text{TileSize}(A) + \text{TileSize}(B) = k_0 + u_0 u_1 \quad (7)$$

<sup>5</sup>Supported optimizations include separated and/or combined read/write bandwidths, varied read and write costs for each tensor, varied quantization for each tensor, additional components such as networks and processing stages (*e.g.*, quantization), heterogeneous compute units (*e.g.*, choose between a MAC array and a scalar engine), and more complex network communication topologies (*e.g.*, multicast and reduction networks).

<sup>6</sup>Tile shape exploration explores bounds for the innermost loop, then the next-innermost of the same rank variable, and so on until this rank variable is exhausted. It then moves to the next-innermost loop for which choices have not been made, and repeats. We have tested this order, finding that this one generally results in the most effective partial tile shape pruning.

The value of  $k_0$  is, while  $u_0, u_1$  are unknown and independent of  $k_0$  (we know the tile size of  $A$  but not  $B$ ). Then GLB usage is minimized if we minimize both  $A$  tile size ( $k_0$ ) and  $B$  tile size ( $u_0 u_1$ ). So, we partition the GLB usage expression into two criteria, one for each term, to be minimized.

However, not all criteria need to be considered, and we can apply another rule: *dropping symbols*. In our example, the criterion  $u_0 u_1$  is completely independent of  $k_0$  and only involves symbols with unknown values. At this point in the exploration, we can ignore  $u_0 u_1$  because we are only pruning choices for  $k_0$ . In general, we partition formulas until they are small enough to either evaluate or drop. We can partition minimizations, maximizations, sums, and products.

Sometimes, there are tile shape interactions that must be included in the criteria we evaluate. For example, if we have enumerated tile shape choices for loop *for*  $x_i$  in  $[0, X_i]$  but not the next-outermost loop of the same rank variable *for*  $x_{i+1}$  in  $[0, X_{i+1}]$ , then choices for  $X_i$  constrain future choices of  $X_{i+1}$  because  $X_i X_{i+1}$  must evenly divide  $X$ . In such cases, we include  $X_i$  as a “cannot compare” criterion such that each  $X_i$  choice yields a different set of  $X_{i+1}$  choices.

Finally, while not listed here for conciseness, there are simple rewrite rules for simplifying expressions such as algebraic simplifications (*e.g.*,  $\frac{k_1 k_2}{k_1} = k_2$ ) and dropping constants (*e.g.*, minimizing  $5x$  is equivalent to minimizing  $x$ ).

## VI. EVALUATION

This section shows that TCM finds the optimal mapping within a feasible runtime. Because TCM always includes choices that can lead to optimal mappings in the searched space, the best mapping found by TCM is optimal. Our first result shows that the pruning and model currying we propose speeds up the exploration enough that TCM finishes within a feasible runtime (*e.g.*, approximately 37 seconds for GPT-3 6.7B). Then, we compare TCM to prior works, showing that the mapping found by TCM has significantly lower EDP (geomean  $2.1\times$ ) given equal runtime budget, and still meaningfully lower EDP (geomean  $1.2\times$ ) even when prior mappers are allowed  $1000\times$  the runtime.

### A. Experiment Setup

TCM supports user-configurable hardware and workload configurations. In this evaluation, we use two workloads and two hardware configurations.

1) *Workloads*: Workloads used are GPT-3 6.7B [6] and MobileNetV3 [19]. GPT-3 workload includes one decoder layer, including embedding, multi-headed self-attention, and feedforward layers. We label the Einsums are as follows.

- $Q, K, V$ : the query, key, and value projection in GPT-3.
- $Z$ : the output projection in GPT-3.
- $QK, AV$ : multi-head attention computation in GPT-3.
- $FFA, FFB$ : feedforward layer in GPT-3.
- $P$ : pointwise convolution in MobileNetV3.
- $D$ : depthwise convolution in MobileNetV3.

Workload	Einsum	# Mappings (orders of magnitude)		
		Total	Non-Pruned	Reduction
<b>GPT-3</b>	V, K, Q, Z	36	7	29
	QK, AV	37	6	30
	FFA, FFB	30	7	22
<b>MobileNetV3</b>	D0	28	5	24
	D1, D2	30	5	25
	P0	21	4	17
	P1, P2	23	4	19

TABLE II

NUMBER OF TOTAL AND NON-PRUNED MAPPINGS THAT MUST BE EVALUATED BY TCM. EINSUMS WITH THE SAME RESULTS ARE ON THE SAME ROW. (e.g., EINSUMS  $V, K, Q$ , AND  $Z$  EACH HAVE  $10^{36}$  MAPPINGS BEFORE PRUNING AND  $10^7$  MAPPINGS AFTER). PRUNING RATE (REDUCTION) INCREASES WITH LARGER MAPSPACES, MAKING THE NUMBER OF NON-PRUNED MAPPINGS ALWAYS TRACTABLE.

2) *Architecture*: GPT-3 workloads are run on a TPU-V4i-like [20], [21] datacenter accelerator, and MobileNetV3 workloads are run on an NVDLA-like [22], [23] edge accelerator. TPU-V4i configuration is taken from the papers, and includes compute energy, access energy of each memory level, and bandwidths of each memory level (including DRAM). It includes a 128MB global buffer and four PEs. Each PE includes a 4MB local buffer and a  $128 \times 128$  array of MACs and registers (holding one weight value each). The array multicasts inputs on one dimension and reduces outputs on the other.

The NVDLA-like configuration is taken from public data [22]. Access energy and bandwidths are modeled using HWComponents [24]–[26]. It includes a 64kb global buffer and a  $32 \times 192$  MAC array that reuses inputs along the 32-long dimension and reduces outputs along the 192-long dimension.

### B. Pruning Rate

Here, we show how each of our optimizations affects the number of mappings that must be evaluated. We show results for GPT-3 6.7B prefill with batch 64 and 65536 tokens. MobileNet-V3 is shown with batch 64.

Table II shows the total number of mappings, the number of unpruned mappings that must be evaluated by TCM, and the reduction. Across Einsums, the mapspace size varies ( $10^{23}$ – $10^{37}$ ) because the number of ranks and the shape of tensors vary. But even for the largest mapspace, TCM produces a tractable number of non-pruned mappings to evaluate (at most  $10^7$  mappings). In fact, across all Einsums, the pruning rate varies between  $10^{19}$ – $10^{30}$ , generally increasing as the size of the mapspace increases.

To show how TCM achieves these pruning rates, Fig. 6 breaks down mapspace size reductions into Tile Shape Pruning, Dataflow Pruning, and Partial Tile Shape Pruning. We can see that Dataflow Pruning is most effective, followed by Tile Shape Pruning, and finally Partial Tile Shape Pruning. All three are essential to make mapspace exploration feasible; the weakest, Partial-Tile-Shape pruning, still reduces search size by up to seven orders of magnitude.

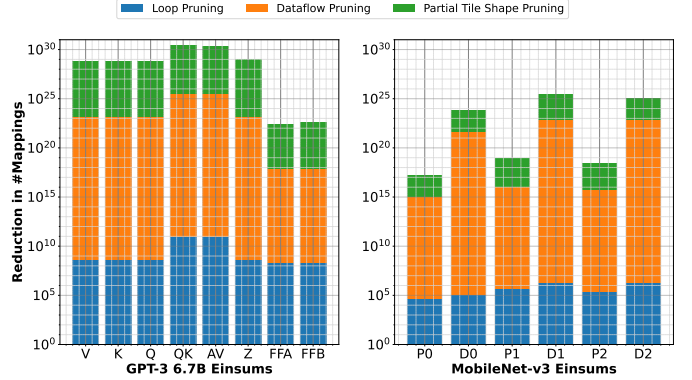


Fig. 6. Search size reduction by each of our optimizations. The Y axis is multiplicative and cumulative. For example, the first bar shows that for Einsum  $V$ , Tile Shape Pruning reduces search size by  $\sim 9$  orders of magnitude, Tile Shape and Dataflow Pruning together reduce search size by  $\sim 28$  orders of magnitude, and all three together reduce search size by  $\sim 29$  orders of magnitude. All optimizations are essential to make this exploration feasible, as each yields an orders-of-magnitude reduction in search size.

### C. Pruning Rate and Mapspace Size

As mapspace size increases, pruning rate increases as well, making TCM effective for exploring even extremely large mapspaces. To show why, Fig. 7 shows how the mapspace size and pruned mapspace size scale for the TPU-v4i-like accelerator running matrix multiplication workload with varied-size matrices and with additional ranks.

As matrix size increases (see Fig. 7, left), the number of tile shapes increases because there are more possible tile shapes. However, after pruning, the number of mappings increases at a much slower rate. This is for two reasons. First, loop pruning, in removing loops, eliminates more tile shape options because it removes the possible bounds for those loops. Then, partial tile shape pruning eliminates more tile shapes early on, because more tile shapes tend to be invalid or suboptimal. The one decrease in the plot– when moving from a matrix size of

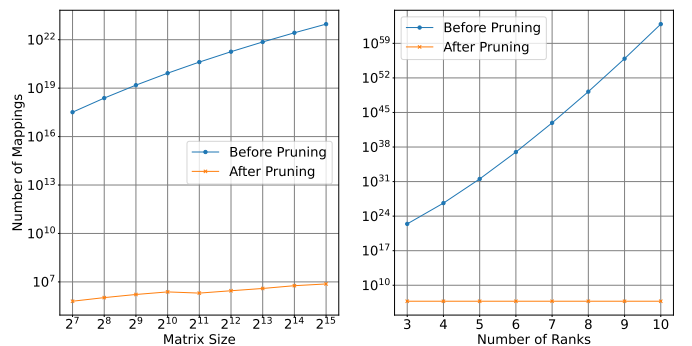


Fig. 7. Mspace size scaling, with and without pruning, for matrix multiplies on a TPU-v4i-like accelerator. (Left) Mspace size scaling as matrix size increases, with three total ranks ( $M, N$ , and  $K$ ). (Right) Mspace size scaling as the number of ranks increases, with matrix dimensions  $M = N = K = 16384$  and additional size-1 ranks added to the weight tensor. As mspace size increases, pruning becomes more effective, keeping search size tractable even for very large mapspaces.

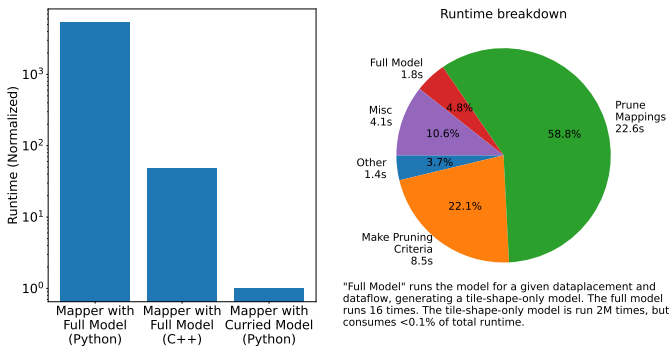


Fig. 8. (Left) Model speed comparison. The curried model reduces runtime by  $40\times$  and  $400\times$  versus full Python and C++ implementations, respectively. (Right) Runtime breakdown with the curried model. The curried model is very fast, that the overall runtime is dominated by other parts of the mapper.

$2^{11}$  to  $2^{12}$ —occurs when the matrices become too large to fit in the TPU-v4i local buffers, and partial tile shape pruning quickly prunes these invalid tile shapes early on.

As the number of ranks increases (right half of Fig. 7), the number of mappings increases as the number of loop orders increases. Each additional loop multiplies the number of dataflows (as the number of loop orders increases with the factorial of the number of elements in a set). However, this growth is entirely prevented by Dataflow Pruning, because we explore dataplaces, not loop orders.

#### D. Runtime with Fast Model

Here, we show how the curried model affects overall runtime. We test GPT-3 Einsum  $QK$ , showing the runtime of TCM while using three different models.

- Full (Python): Our model without currying. This model is a basic, non-optimized Python implementation.
- Full (C++): An optimized C++ implementation from Timeloop [1].
- Curried: Our two-step curried model, written in Python. It is first partially evaluated only with dataflow and dataplacement (16 times), then is partially evaluated (2M times) with tile shapes.

Fig. 8 shows the runtime of the full TCM while using each model for all evaluations. We see that the curried model is significantly faster than the C++ and Python models, reducing runtime by  $40\times$  and  $400\times$ , respectively.

Fig. 8 shows the runtime breakdown; with currying, the model is fast enough that runtime is suboptimal by making pruning criteria (Section V-D) and pruning mappings. Partial evaluation of the model for each dataplacement and dataflow, occurring 16 times in this experiment, consumes < 5% of the runtime. Finally, the tile-shape-only model, which has been partially evaluated (going from thousands of lines of Python to a handful of sum-of-product and max expressions), consumed < 0.1% of runtime, despite being called two million times.

#### E. Comparison with prior works

In this subsection, we compare against prior mappers. We run GPT-3 6.7B Einsum  $QK$  on TPU-V4i-like with batch size

Runtime	Best EDP (normalized) found when given runtime			
	$t_0$	$10 \times t_0$	$100 \times t_0$	$1000 \times t_0$
Timeloop	2399	463	192	6.08
Timeloop + Hint	3.05	3.05	3.00	2.88
LOMA	1.28	1.28	1.28	1.21
TCM	1			Completed

TABLE III  
EDP COMPARISON OF TCM AND PRIOR MAPPERS GIVEN VARIOUS RUNTIMES (LOWER IS BETTER). TCM FINDS AN OPTIMAL MAPPING IN  $t_0 = 37$  SECONDS. PRIOR MAPPERS FAIL TO CONVERGE EVEN WHEN GIVEN  $1000 \times$  THE RUNTIME ( $> 10$  HOURS).

64 and 65,536 tokens. We compare to the following mappers:

- **Timeloop** [1] is a commonly used prior mapper that uses random sampling to explore the mapspace.
- **Timeloop+Hint** reflects a common use case of Timeloop, in which users define mapspace constraints to speed up mapping. We implement a common constraint: the mapping must spatially utilize the full MAC arrays.
- **LOMA**, integrated into the ZigZag [7] framework, first creates tile shapes, then explores dataflows and dataplaces for these shapes. LOMA constrains mappings to fully utilize PEs and MACs (like Timeloop+Hint).

We note that the full-utilization constraints in Timeloop+Hint and LOMA are not guaranteed to be optimal (e.g., would yield only invalid mappings if the MAC array is very large and needs tiles too large for the local buffer). However, in this particular case, these constraints preserve the known mapping (found by TCM).

We first run TCM to completion ( $\sim 37$  seconds). We run Timeloop given various timeouts and report the best mapping found. LOMA results are generated by varying LOMA’s LPF setting (described in [9]), which constrains tile shape choices to reduce runtime. We report the best mapping found by LOMA in the most comprehensive mapspace (highest LPF setting) that finishes within each time limit. Because LOMA can only run single-threaded, for fairness, we also only use one thread for TCM and Timeloop (both of which can parallelize).

Table III compared the best EDP found. Within TCM’s runtime ( $t_0$ ), all baselines are far from optimal. Timeloop, which samples randomly, has a very high EDP because of severe underutilization of the MAC array (tile shapes that perfectly utilize the array shape are rare). Timeloop+Hint has significantly better EDP, but still picks poor dataflows and tile shapes, often increasing energy and/or latency with excessive off-chip fetches. LOMA quickly achieves a fair EDP ( $1.28 \times$  optimal) because it includes additional heuristics (always fully utilize spatial units, optimize accesses for one level at a time); however, it improves only marginally with more runtime.

We note that TCM also guarantees optimality, while Timeloop and LOMA can only do so with full exploration of the mapspace (which would require an infeasible additional  $> 10^{20} \times$  additional runtime).

## VII. CONCLUSION

In this paper, we have shown the important new concept of *dataplacement*, which, alongside dataflow and tile shapes, provides a clear way to understand and analyze mappings. Defining and decoupling dataplacement lets us perform new mapping analyses, letting us identify and prune suboptimal choices and create a much more efficient curried model. We show that these improvements make it possible, for the first time, to fully explore mapspaces and find optimal mappings.

## REFERENCES

- [1] A. Parashar, P. Raina, Y. S. Shao, Y.-H. Chen, V. A. Ying, A. Mukkara, R. Venkatesan, B. Khailany, S. W. Keckler, and J. Emer, “Timeloop: A systematic approach to dnn accelerator evaluation,” in *2019 IEEE International Symposium on Performance Analysis of Systems and Software (ISPASS)*, 2019, pp. 304–315.
- [2] H. Kwon, P. Chatarasi, V. Sarkar, T. Krishna, M. Pellauer, and A. Parashar, “Maestro: A data-centric approach to understand reuse, performance, and hardware cost of dnn mappings,” *IEEE Micro*, vol. 40, no. 3, pp. 20–29, 2020.
- [3] S. Zheng, S. Chen, S. Gao, L. Jia, G. Sun, R. Wang, and Y. Liang, “Tileflow: A framework for modeling fusion dataflow via tree-based analysis,” in *Proceedings of the 56th Annual IEEE/ACM International Symposium on Microarchitecture*, ser. MICRO ’23. New York, NY, USA: Association for Computing Machinery, 2023, p. 1271–1288. [Online]. Available: <https://doi.org/10.1145/3613424.3623792>
- [4] J. Cai, Y. Wei, Z. Wu, S. Peng, and K. Ma, “Inter-layer scheduling space definition and exploration for tiled accelerators,” in *Proceedings of the 50th Annual International Symposium on Computer Architecture*, ser. ISCA ’23. New York, NY, USA: Association for Computing Machinery, 2023. [Online]. Available: <https://doi.org/10.1145/3579371.3589048>
- [5] M. Gilbert, Y. N. Wu, J. S. Emer, and V. Sze, “Looptree: Exploring the fused-layer dataflow accelerator design space,” *IEEE Transactions on Circuits and Systems for Artificial Intelligence*, vol. 1, no. 1, pp. 97–111, 2024.
- [6] T. Brown, B. Mann, N. Ryder, M. Subbiah, J. D. Kaplan, P. Dhariwal, A. Neelakantan, P. Shyam, G. Sastry, A. Askell, S. Agarwal, A. Herbert-Voss, G. Krueger, T. Henighan, R. Child, A. Ramesh, D. Ziegler, J. Wu, C. Winter, C. Hesse, M. Chen, E. Sigler, M. Litwin, S. Gray, B. Chess, J. Clark, C. Berner, S. McCandlish, A. Radford, I. Sutskever, and D. Amodei, “Language Models are Few-Shot Learners,” in *Advances in Neural Information Processing Systems*, vol. 33. Curran Associates, Inc., 2020, pp. 1877–1901. [Online]. Available: <https://papers.nips.cc/paper/2020/hash/1457e0d6bfc4967418bfb8ac142f64a-Abstract.html>
- [7] L. Mei, P. Houshmand, V. Jain, S. Giraldo, and M. Verhelst, “Zigzag: Enlarging joint architecture-mapping design space exploration for dnn accelerators,” *IEEE Transactions on Computers*, vol. 70, no. 8, pp. 1160–1174, 2021.
- [8] M. Olyaiy, C. Ng, A. S. Fedorova, and M. Lis, “Sunstone: A scalable and versatile scheduler for mapping tensor algebra on spatial accelerators,” in *2023 IEEE International Symposium on Performance Analysis of Systems and Software (ISPASS)*, 2023, pp. 259–271.
- [9] A. Symons, L. Mei, and M. Verhelst, “Loma: Fast auto-scheduling on dnn accelerators through loop-order-based memory allocation,” in *2021 IEEE 3rd International Conference on Artificial Intelligence Circuits and Systems (AICAS)*, 2021, pp. 1–4.
- [10] Q. Huang, M. Kang, G. Dinh, T. Norell, A. Kalaiah, J. Demmel, J. Wawrzynek, and Y. S. Shao, “Cosa: Scheduling by constrained optimization for spatial accelerators,” in *2021 ACM/IEEE 48th Annual International Symposium on Computer Architecture (ISCA)*, 2021, pp. 554–566.
- [11] Chen, Yu-Hsin and Krishna, Tushar and Emer, Joel and Sze, Vivienne, “Eyeriss: An Energy-Efficient Reconfigurable Accelerator for Deep Convolutional Neural Networks,” in *IEEE International Solid-State Circuits Conference, ISSCC 2016, Digest of Technical Papers*, 2016, pp. 262–263.
- [12] V. Sze, Y.-H. Chen, T.-J. Yang, and J. S. Emer, “Efficient processing of deep neural networks,” *Synthesis Lectures on Computer Architecture*, vol. 15, no. 2, pp. 1–341, 2020. [Online]. Available: <https://doi.org/10.2200/S01004ED1V01Y202004CAC050>
- [13] M. Gilbert, “Looptree: Enabling systematic and flexible exploration of fused-layer dataflow accelerators,” PhD thesis, University of Example, Example City, CA, November 2023, available at <https://example.com/thesis.pdf>.
- [14] S.-C. Kao and T. Krishna, “Gamma: Automating the hw mapping of dnn models on accelerators via genetic algorithm,” in *2020 IEEE/ACM International Conference On Computer Aided Design (ICCAD)*, 2020, pp. 1–9.
- [15] C. Sakhija, Z. Shi, and C. Lin, “Leveraging domain information for the efficient automated design of deep learning accelerators,” in *2023 IEEE International Symposium on High-Performance Computer Architecture (HPCA)*, 2023, pp. 287–301.
- [16] Z. Jia, M. Zaharia, and A. Aiken, “Beyond data and model parallelism for deep neural networks,” in *Proceedings of Machine Learning and Systems*, A. Talwalkar, V. Smith, and M. Zaharia, Eds., vol. 1, 2019, pp. 1–13. [Online]. Available: [https://proceedings.mlsys.org/paper\\_files/paper/2019/file/b422680f3db0986ddd7f8f126baaf0fa-Paper.pdf](https://proceedings.mlsys.org/paper_files/paper/2019/file/b422680f3db0986ddd7f8f126baaf0fa-Paper.pdf)
- [17] Y.-H. Chen, J. Emer, and V. Sze, “Eyeriss: A spatial architecture for energy-efficient dataflow for convolutional neural networks,” in *2016 ACM/IEEE 43rd Annual International Symposium on Computer Architecture (ISCA)*, 2016, pp. 367–379.
- [18] M. Alwani, H. Chen, M. Ferdman, and P. Milder, “Fused-layer cnn accelerators,” in *2016 49th Annual IEEE/ACM International Symposium on Microarchitecture (MICRO)*, 2016, pp. 1–12.
- [19] A. Howard, M. Sandler, B. Chen, W. Wang, L.-C. Chen, M. Tan, G. Chu, V. Vasudevan, Y. Zhu, R. Pang, H. Adam, and Q. Le, “Searching for mobilenetv3,” in *2019 IEEE/CVF International Conference on Computer Vision (ICCV)*, 2019, pp. 1314–1324.
- [20] N. P. Jouppi, C. Young, N. Patil, D. Patterson, G. Agrawal, R. Bajwa, S. Bates, S. Bhatia, N. Boden, A. Borchers, R. Boyle, P.-l. Cantin, C. Chao, C. Clark, J. Coriell, M. Daley, M. Dau, J. Dean, B. Gelb, T. V. Ghaemmaghami, R. Gottipati, W. Gulland, R. Hagmann, C. R. Ho, D. Hogberg, J. Hu, R. Hundt, D. Hurt, J. Ibarz, A. Jaffey, A. Jaworski, A. Kaplan, H. Khaitan, D. Killebrew, A. Koch, N. Kumar, S. Lacy, J. Laudon, J. Law, D. Le, C. Leary, Z. Liu, K. Lucke, A. Lundin, G. MacKean, A. Maggiore, M. Mahony, K. Miller, R. Nagarajan, R. Narayanaswami, R. Ni, K. Nix, T. Norrie, M. Omernick, N. Penukonda, A. Phelps, J. Ross, M. Ross, A. Salek, E. Samadiani, C. Severn, G. Sizikov, M. Snelham, J. Souter, D. Steinberg, A. Swing, M. Tan, G. Thorson, B. Tian, H. Toma, E. Tuttle, V. Vasudevan, R. Walter, W. Wang, E. Wilcox, and D. H. Yoon, “In-datacenter performance analysis of a tensor processing unit,” in *2017 ACM/IEEE 44th Annual International Symposium on Computer Architecture (ISCA)*, 2017, pp. 1–12.
- [21] N. P. Jouppi, D. Hyun Yoon, M. Ashcraft, M. Gottsch, T. B. Jablin, G. Kurian, J. Laudon, S. Li, P. Ma, X. Ma, T. Norrie, N. Patil, S. Prasad, C. Young, Z. Zhou, and D. Patterson, “Ten lessons from three generations shaped google’s tpu4i : Industrial product,” in *2021 ACM/IEEE 48th Annual International Symposium on Computer Architecture (ISCA)*, 2021, pp. 1–14.
- [22] Nvidia deep learning accelerator. [Online]. Available: <http://nvdla.org/primer.html>
- [23] NVIDIA. (2025) NVIDIA DGX B200. Accessed: August 1, 2025. [Online]. Available: <https://www.nvidia.com/en-us/data-center/dgx-b200/>
- [24] T. Andrusis, J. S. Emer, and V. Sze, “CiMLoop: A flexible, accurate, and fast compute-in-memory modeling tool,” in *2024 IEEE International Symposium on Performance Analysis of Systems and Software (ISPASS)*, 2024, pp. 10–23.
- [25] Y. N. Wu, J. S. Emer, and V. Sze, “Accelergy: An architecture-level energy estimation methodology for accelerator designs,” in *2019 IEEE/ACM International Conference on Computer-Aided Design (ICCAD)*, 2019, pp. 1–8.
- [26] S. Thozhiyoor, J. H. Ahn, M. Monchiero, J. B. Brockman, and N. P. Jouppi, “A comprehensive memory modeling tool and its application to the design and analysis of future memory hierarchies,” in *2008 International Symposium on Computer Architecture*, 2008, pp. 51–62.